Shock Resistive Flexure-Based Anthropomorphic Hand with Enhanced Payload

Article *in* Soft Robotics · March 2021

DOI: 10.1089/soro.2020.0067

4 authors, including:

Junmo Yang
Daegu Gyeongbuk Institute of Science and Technology
4 PUBLICATIONS **4** CITATIONS

SOFT ROBOTICS
Volume 00, Number 00, 2021

DOI: 10.1089/soro.2020.0067

SoRo
Soft Robotics

Shock Resistive Flexure-Based Anthropomorphic Hand with Enhanced Payload

Junmo Yang,* Jeongseok Kim,* Donghyun Kim, and Dongwon Yun

Abstract

In this study, a Crossed Flexural Hinge (CFH) structure was used for the design of a humanoid robot hand that can absorb any abrupt external force and that has a large payload, giving it the advantages of both rigid and compliant robots. Structural problems were identified through a 6×6 stiffness matrix to analyze whether CFH is suitable for use as an anthropomorphic robot hand. To reinforce the weak stiffness, a paired CFH (p-CFH) structure was proposed for the robot hand joints. In addition, it was verified through theoretical and experimental methods that p-CFH has superior stiffness characteristics compared to conventional CFH. When designing the anthropomorphic robot hand, p-CFH was appropriately deformed and applied. Using an underactuated wire mechanism suitable for the structure of the robot hand, it was possible to grasp objects of various shapes in a shape-adaptive manner. It was confirmed that the final anthropomorphic robot hand was able to stably hold an object of an unspecified shape without precisely controlling the motor. And the robot hand can also hold a heavy object due to the increased rigidity of the p-CFH. In addition, by conducting the qualitative impact test in which the robot was subjected to an impact in an arbitrary direction, it was confirmed that the robot, due to compliance of the joints, can absorb impact without incurring damage. Finally, a quantitative impact test was conducted in all directions, and the shock absorbing capability of anthropomorphic robot hand was verified through numerical comparison with the control model.

Keywords: soft hand robot, cross flexure hinge, anthropomorphic hand robot, shock resistive robot

Introduction

Pin joints, or revolute joints, are kinematic pairs that constrain the relative motion of two different links to rotational motion with one-degree-of-freedom (1-DOF). Structures in which rigid links are connected by pin joints have several structural strengths. In particular, most small grippers use pin joints. In a small gripper, the motor cannot be attached to individual links, so the wire actuation method is used, and the most suitable structure for such wire actuation is a pin joint.[1] These joints also have the advantage of being able to withstand vertical force on the finger.[2] Structures in which rigid links are connected by pin joints have been frequently used in the design of robot hands due to the advantages of easy kinematic analysis, high mechanical strength, and stiffness, which can withstand high loads.[3,4] Because they can easily imitate human hand joints, including metacarpophalangeal, proximal interphalangeal, and distal interphalangeal joint structures, pin joints are also used in the manufacture of anthropomorphic hands.[5] However, since the components are not compliant materials, and they may be susceptible to impacts in unspecified directions, it is difficult to adapt pin joints to the environment, and there are disadvantages in that the assembly is complicated due to the large number of parts.

To compensate for the shortcomings of the rigid pin joint-based robot hand, research has been conducted on a compliant robot hand that holds an object using elastic deformation of a flexible material. Compliant hands are divided into two types as follows: a fully-compliant robot hand in which elastic deformation occurs in the entire robot hand, and a partially-compliant robot hand in which deformation occurs only in a specific part. When manufacturing a fully-compliant robot hand, a method of pouring silicone into a mold is

Department of Robotics Engineering, Daegu Gyeongbuk Institute of Science and Technology (DGIST), Daegu, South Korea.
*These authors contributed equally to this work.

typically used. In studies using silicon to develop robot hands, there have been studies designed to create a chamber within one finger to move three fingers[6] and studies in which three to five fingers are implemented.[7–9] There is a study to realize the desired elasticity by changing the thickness of the silicon finger and a previous study to suggest a finger with tunable joint stiffness by combining tendon and pneumatic actuation schemes.[10,11] If the robot is made of a flexible material such as silicon, it can absorb external disturbances structurally due to the inherent compliance of the material and can use a deformable body to catch various objects in a shape-adaptive method without complicated control. In addition, there is an advantage in that the assembly process can be minimized using the mold to make the robot as a single body. However, fully compliant robot hands have a disadvantage in that the load that can be gripped is relatively low and, due to its low mechanical rigidity, the hand is easily damaged by sharp objects compared to rigid-pin joint robot hands. Another disadvantage is that if the body of the robot is manufactured as a single body using a silicone mold, there is a possibility that the entire body will have to be manufactured again, even if it is only partially damaged.

When manufacturing a partially compliant robot hand, a method of connecting a rigid link with a flexure hinge is used. Flexure hinges have been used as mechanical elements to replace existing rolling bearings because they have a property of being deformed only in a specific direction because their rigidity depends on direction. Unlike rolling bearings, in which friction between elements occurs continuously, flexure hinges utilize monolithic elastic deformation. Therefore, a flexure does not generate friction while operating, and so no lubrication is required and no backlash occurs, allowing more precise movement. Because of these advantages, flexure hinges have been used in many studies such as precision machinery,[12,13] a gripper for micro units,[14] and high-precision stages.[15,16] Flexure hinges have been utilized in the design of robot hands,[17] because they can act as joints, springs, and dampers at the same time, enabling compact design. Odhner *et al.* used flexure hinges to create a robot hand that could hold various objects in firm power grasp and low-stiffness fingertip grasp methods.[18] As described above, since the mechanical properties of the flexure hinge vary depending on the shape and material, it is very important to select and design the most suitable flexure for the operating characteristics of the mechanical system.

Crossed Flexural Hinge (CFH) is a structure that is frequently used as a 1-DOF revolute joint. As shown in Figure 1a, the most basic CFH is arranged in parallel at the twisted position of two rectangular thin beams, so that the two links above and below are connected. CFH has low stiffness to the moment applied to the z-axis and high stiffness to the axial load applied along the z-axis. (In the following context, the resistance to the line load in the z-axis direction applied to the link is indicated as supporting stiffness.) The design of CFH applied according to the type of mechanical system should be different. Several studies have presented a method to select design parameters such as the length, angle, and width of a CFH beam and a mechanical analysis method to identify the mechanical properties of CFH.[19–23]

In this study, a CFH structure was used to design an anthropomorphic robot hand that has both the shock absorbing capability of a compliant robot and the high load carrying capability of a rigid robot. When CFH is applied to a robot hand, it is possible to express the bending of a finger by performing a rotational movement of the joint. In addition, since the rigidity is large in a direction perpendicular to the plane of rotation, the load of the object can be

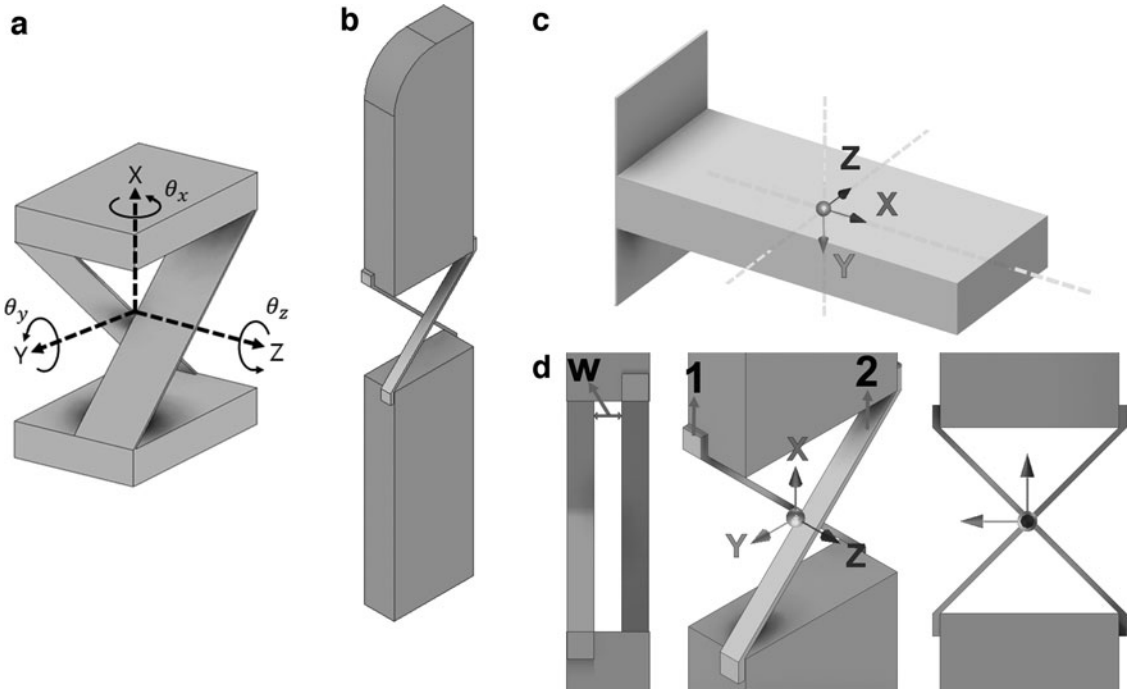

FIG. 1. Coordinates and an application of CFH. **(a)** Coordinate of 1 p-CFH. It rotates along z-axis. **(b)** A finger joint made by 1 p-CFH. **(c)** Cantilever beam with coordinate. **(d)** Design of CFH. CFH, Crossed Flexural Hinge; p-CFH, paired CFH.

supported when the robot hand grasps the object. In the first study to apply CFH to a robot hand, a robot finger using CFH was proposed, and kinematic analysis of the robot hand was performed in two-dimensions (2D) using the Pseudo Rigid Body model and Virtual work method.[24] However, the 2D analysis of that article is difficult to use for verification of the effectiveness of CFH for a humanoid robot hand that uses a grabbing motion in three-dimensions (3D). Creating a robot hand usually requires a large number of joints. Unlike a rolling bearing, if a flexure hinge that inevitably behaves in 3D is used often, 3D microdeformation occurs at each hinge when holding the object. This results in large deformations throughout the robot hand. For this reason, there is a possibility that it cannot properly grasp; 3D analysis is essential to overcome this problem. Therefore, we analyzed the CFH joint using a 3D stiffness matrix of CFH and proposed a paired CFH (p-CFH) joint for the robot hand to effectively eliminate the out-of-plane compliance component that makes the fingers twist when the robot hand grasps the object. Rigidity analysis was also conducted on the newly proposed model, and it was confirmed that out-of-plane compliance was effectively eliminated, and that hand had a load carrying capacity better compared with the existing CFH. When applying the p-CFH model used in the theoretical analysis to an anthropomorphic robot hand, we analyzed the various problems that could be expected and applied an appropriately modified shape of the p-CFH to solve any problems. Finally, a four-finger type anthropomorphic robot hand prototype was developed to carry out an experiment of catching objects of various shapes and weights, and a payload test using cylindrical object was conducted to confirm that hand had the desired level of compliance and load carrying capacity. In addition, it was confirmed through the quantitative and qualitative impact test that the robot hand can withstand the impact.

Stiffness Analysis of CFH

First, to analyze the stiffness characteristics of CFH joints, we derived a 3D stiffness matrix of CFH based on existing research.[25] The CFH model used in the calculation is shown in Figure 1d. As can be seen in the figure, the CFH connects two finger links. For ease of calculation of the stiffness matrix, the beam is made at an angle of 45° to the y-axis, and a distance of w is provided to prevent friction between the two beams when the finger is bent. The method of obtaining the CFH stiffness matrix is introduced in detail in a related study. The force and moment applied to an arbitrary point on a 3D structure are expressed by multiplying the stiffness matrix by the displacement matrix. The 6×6 stiffness matrix "$k_{cantilever}$" of local coordinates located at the center of gravity of the cantilever beam in Figure 1c is expressed as follows:

$$\begin{bmatrix} F_x \\ F_y \\ F_z \\ M_x \\ M_y \\ M_{xz} \end{bmatrix} = \begin{bmatrix} k_{F_x,x} & 0 & 0 & 0 & 0 & 0 \\ 0 & k_{F_y,y} & 0 & 0 & 0 & 0 \\ 0 & 0 & k_{F_z,z} & 0 & 0 & 0 \\ 0 & 0 & 0 & k_{M_x,\theta_x} & 0 & 0 \\ 0 & 0 & 0 & 0 & k_{M_y,\theta_y} & 0 \\ 0 & 0 & 0 & 0 & 0 & k_{M_y,\theta_y} \end{bmatrix} \begin{bmatrix} x \\ y \\ z \\ \theta_x \\ \theta_y \\ \theta_z \end{bmatrix} \tag{1}$$

$$\begin{bmatrix} k_{F_x,x} & k_{F_y,y} & k_{F_z,z} \\ k_{M_x,\theta_x} & k_{M_y,\theta_y} & k_{M_z,\theta_z} \end{bmatrix} = E \begin{bmatrix} \left(\frac{hb}{L}\right) & \left(\frac{bh^3}{L^3}\right) & \left(\frac{hb^3}{L^3}\right) \\ \left(\frac{bh^3}{L^3}\right)\left(\frac{1}{6(1+\nu)}\right) & \left(\frac{hb^3}{12L}\right) & \left(\frac{bh^3}{12L}\right) \end{bmatrix} = E \begin{bmatrix} S_{F_x} & S_{F_y} & S_{F_z} \\ S_{M_x} & S_{M_y} & S_{M_z} \end{bmatrix} \tag{2}$$

In Eq. (2), E is the modulus of elasticity, ν is Poisson's ratio, L is the length of the beam, and b and h are the width and height of the beam, respectively. The values expressed as fractions expressing stiffness in the matrix of Eq. (2) are expressed as $S_{N\left(N=F_x,\ F_y,\ F_z,\ M_x, M_y,\ M_z\right)}$ after excluding the commonly multiplied E. For example, when calculating $k_{F_y,y}$, beam deflection in the y-axis direction can be expressed as $y(L)\cong\frac{F_yL^3}{12EI_z}$ according to cantilever beam bending equation. The linear stiffness along the y-axis can be divided by the deflection of the applied force, so $k_{F_y,y}=\frac{F_y}{y(L)}\cong\frac{12EI_z}{L^3}=E\left(\frac{bh^3}{L^3}\right)$. And the angular stiffness k_{M_x,θ_x} is expressed as the product of Coulomb modulus G and polar moment of inertia J divided by L. Therefore, $k_{M_x,\theta_x}=\frac{GJ}{L}=\frac{1}{3}\left(\frac{bh^3}{L^3}\right)\left(\frac{1}{2(1+\nu)}\right)$. k_{M_z,θ_z} and k_{M_y,θ_y} can be obtained by $\frac{EI_y}{L}$ and $\frac{EI_z}{L}$, respectively, so it is expressed as $\left[\left(\frac{E}{12}\right)\left(\frac{bh^3}{L}\right)\right]$ and $\left[\left(\frac{E}{12}\right)\left(\frac{hb^3}{12L}\right)\right]$. Detailed information on each term can be found in the part ① of Supplementary Data. For more interested readers are directed to reference, Yves Bellouard.[25] The stiffness matrix at point O located at the center of the two links of CFH, shown in Figure 1d, can be obtained using the stiffness matrix of the cantilever beam. Assuming that the transformation matrix moving from the local coordinate of beam 1 to point O is $T_{1\to O}$, and the transformation matrix moving from the local coordinate of beam 2 to point O is $T_{2\to O}$, k_{CFH}, which is stiffness matrix of CFH at point O, can be presented as

$$k_{CFH}=(T_{1\to O})k_{cantilever}(T_{1\to O})^T+\ (T_{2\to O})k_{cantilever}(T_{2\to O})^T \tag{3}$$

In Eq. (3), $T_{1\to O}$ denotes the transformation matrix that rotates the stiffness matrix of beam 1 by –45° on the z-axis and then translates it parallel by $+\frac{b+w}{2}$. The value of $+\frac{b+w}{2}$ can be expressed as P_1. $T_{2\to O}$ denotes the transformation matrix that rotates the stiffness matrix of beam 2 by 45° on the z-axis and translates it parallel by $-P_1$. The obtained transformation matrix is expressed as follows:

$$T_{1\to O}=\begin{bmatrix} C_{\pi/4} & S_{\pi/4} & 0 & 0 & 0 & 0 \\ -S_{\pi/4} & C_{\pi/4} & 0 & 0 & 0 & 0 \\ 0 & 0 & 1 & 0 & 0 & 0 \\ 0 & P_1 & 0 & C_{\pi/4} & S_{\pi/4} & 0 \\ -P_1 & 0 & 0 & -S_{\pi/4} & C_{\pi/4} & 0 \\ 0 & 0 & 0 & 0 & 0 & 1 \end{bmatrix} \tag{4}$$

$$T_{2\to O}=\begin{bmatrix} C_{\pi/4} & -S_{\pi/4} & 0 & 0 & 0 & 0 \\ S_{\pi/4} & C_{\pi/4} & 0 & 0 & 0 & 0 \\ 0 & 0 & 1 & 0 & 0 & 0 \\ 0 & -P_1 & 0 & C_{\pi/4} & -S_{\pi/4} & 0 \\ P_1 & 0 & 0 & S_{\pi/4} & C_{\pi/4} & 0 \\ 0 & 0 & 0 & 0 & 0 & 1 \end{bmatrix} \quad (5)$$

In Eqs. (4) and (5), $C_{\pi/4}$ and $S_{\pi/4}$ mean $\cos\left(\frac{\pi}{4}\right)$ and $\sin\left(\frac{\pi}{4}\right)$, respectively. The stiffness matrix k_{CFH} obtained by multiplying the stiffness matrix in Eq. (1) by the transformation matrices in Eqs. (4) and (5), respectively, can be presented as follows:

$$k_{CFH}=\begin{bmatrix} k_{F_x,x} & 0 & 0 & k_{F_x,\theta_x} & 0 & 0 \\ 0 & k_{F_y,y} & 0 & 0 & k_{F_y,\theta_y} & 0 \\ 0 & 0 & k_{F_z,z} & 0 & 0 & 0 \\ k_{M_x,x} & 0 & 0 & k_{M_x,\theta_x} & 0 & 0 \\ 0 & k_{M_y,y} & 0 & 0 & k_{M_y,\theta_y} & 0 \\ 0 & 0 & 0 & 0 & 0 & k_{M_y,\theta_y} \end{bmatrix} \quad (6)$$

$$\begin{bmatrix} k_{F_x,x} & k_{M_x,\theta_x} \\ k_{F_y,y} & k_{M_y,\theta_y} \\ k_{F_z,z} & k_{M_z,\theta_z} \end{bmatrix} = E\begin{bmatrix} S_{F_x}+S_{F_y} & S_{M_y}+S_{M_x}L^2+2S_{F_y}P_1^2 \\ S_{F_x}+S_{F_y} & S_{M_y}+S_{M_x}L^2+2S_{F_x}P_1^2 \\ 2S_{F_z} & 2S_{M_z} \end{bmatrix} \quad (7)$$

$$\begin{bmatrix} k_{F_x,\,\theta_x} & k_{M_x,\,x} \\ k_{F_y,\,\theta_y} & k_{M_y,\,y} \end{bmatrix} = E\begin{bmatrix} \sqrt{2}S_{F_y}P_1 & \sqrt{2}S_{F_y}P_1 \\ \sqrt{2}S_{F_x}P_1 & \sqrt{2}S_{F_x}P_1 \end{bmatrix} \quad (8)$$

The values for each element belonging to Eq. (6) expressing the stiffness matrix of CFH can be expressed as Eqs. (7) and (8). Eq. (7) includes diagonal elements, and Eq. (8) shows off-diagonal elements. The parameters belonging to each element are the same as for the previous cantilever beam.

The presence of off-diagonal elements means that when a load or moment is applied, displacement occurs in an unintended direction. In this case, when a robot hand is manufactured using CFH, the finger may be twisted by a contact force in the action of holding an object and, thus, may not be able to grasp properly. The torsion can be constrained by adding a beam which has been done in many previous studies.[13,26,27] In those previous studies, a simple mechanism was proposed, but there was a disadvantage in that it was difficult to drive the robot finger due to the complicated arrangement of beams. Therefore, we added an additional CFH that is symmetrically mirrored with respect to the xy-plane, as shown in Figure 2, to improve the driving mechanism by eliminating undesired compliance. In the following sections, this structure is called the p-CFH. The stiffness matrix for the p-CFH can be obtained using the principle of calculating the stiffness matrix of CFH. In other words, the stiffness matrix of the p-CFH can be obtained by unifying the coordinate systems of the four beams constituting the p-CFH and summing each stiffness matrix. By multiplying the matrices of beams 1, 2, 3, and 4 by the transformation matrix and summing them, the stiffness matrix k_{CFH2} of p-CFH at point O can be obtained, as follows:

$$\begin{aligned} k_{CFH2} = {} & (T_{1\to O})k_{cantilever}(T_{1\to O})^T + (T_{2\to O})k_{cantilever}(T_{2\to O})^T \\ & + (T_{3\to O})k_{cantilever}(T_{3\to O})^T + (T_{4\to O})k_{cantilever}(T_{4\to O})^T \end{aligned} \quad (9)$$

The stiffness matrix of the p-CFH obtained by Eq. (9) and the values of its components are as follows:

$$k_{CFH2}=\begin{bmatrix} k_{F_x,x} & 0 & 0 & 0 & 0 & 0 \\ 0 & k_{F_y,y} & 0 & 0 & 0 & 0 \\ 0 & 0 & k_{F_z,z} & 0 & 0 & 0 \\ 0 & 0 & 0 & k_{M_x,\theta_x} & 0 & 0 \\ 0 & 0 & 0 & 0 & k_{M_y,\theta_y} & 0 \\ 0 & 0 & 0 & 0 & 0 & k_{M_y,\theta_y} \end{bmatrix} \quad (10)$$

$$\begin{bmatrix} k_{F_x,x} & k_{M_x,\theta_x} \\ k_{F_y,y} & k_{M_y,\theta_y} \\ k_{F_z,z} & k_{M_z,\theta_z} \end{bmatrix} = 2E\begin{bmatrix} S_{F_x}+S_{F_y} & S_{M_y}+S_{M_x}L^2+S_{F_y}P_2 \\ S_{F_x}+S_{F_y} & S_{M_y}+S_{M_x}L^2+S_{F_x}P_2 \\ 2S_{F_z} & 2S_{M_z} \end{bmatrix} \quad (11)$$

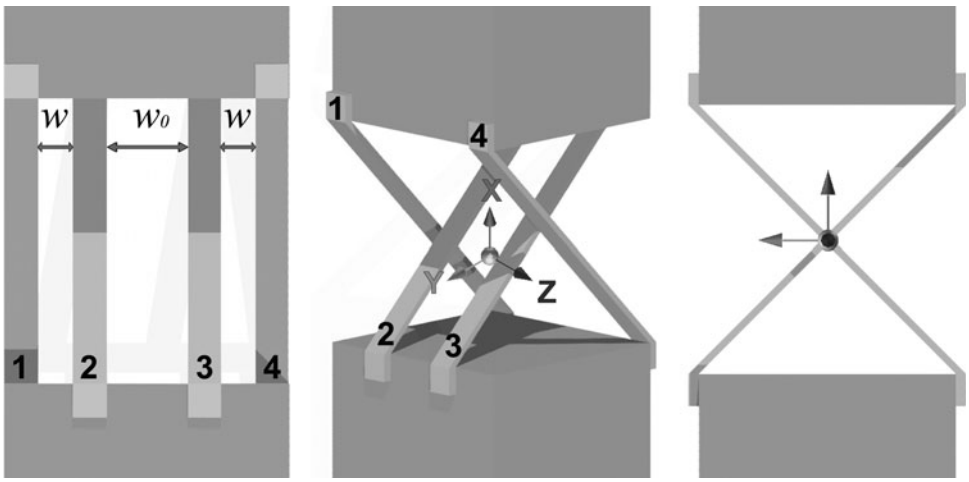

FIG. 2. Design of p-CFH.

In Eq. (11), the parameters belonging to each component are the same as in the previous cantilever beam. The w_o is the distance between the second and third beams, and P_2 means $\left(\frac{3b+w_o}{2}+w\right)^2+\left(\frac{b+w_o}{2}\right)^2$. When the p-CFH is formed by attaching CFH in mirror symmetry, all off-diagonal elements disappear and the diagonal elements change. The amount of change of each element was analyzed. Since it is difficult to determine the ratio of how much stiffness increases in the parameterized state, the stiffness was compared numerically using each parameter with specific values. As shown in Figure 3a, a set of single finger experiments connected by p-CFH was constructed. Values such as the actual height, length, and thickness of this single finger were used in Eq. (12) to obtain the stiffness. The fingers were produced using a resin 3D printer (Formlabs, Somerville, MA) and made of a hollow structure to prevent sagging due to device's own mass. The CFH was manufactured using a stainless steel plate (SUS306) and fixed using screws. From the experimental set, it was confirmed that L is 45.96mm, b is 4.6mm, h is 0.2mm, w is 1.5mm, and w_o is 8.6mm. It can be seen in Eq. (12) that the $k_{M_y,\,\theta_y}$ of the p-CFH is derived and found to be 20.28 times larger compared with the simple CFH as a result of calculation involving substituting the numerical value into the diagonal component, as plotted and compared in Figure 3c. The slope of each graph shows the stiffness of each joint in this figure.

$$\frac{k_{CFH2\_M_y,\theta_y}}{k_{CFH\_M_y,\theta_y}}=\frac{2\left(S_{M_y}+S_{M_x}L^2+S_{F_x}P_2\right)}{S_{M_y}+S_{M_x}L^2+2S_{F_x}P_1^2}\simeq 20.28 \qquad (12)$$

When a robot hand is made with p-CFH, the load of the object applied to the finger link acts as a moment M_y with respect to the center point of CFH. The value k_{M_y,θ_y}, which is the stiffness of a rotational direction, and moment M_y are an important component that indicates the load carrying capacity of the robot hand. Next, the stiffness difference obtained theoretically was verified through experiments. When conducting the experiment, it is impossible to directly apply M_y to point O of CFH and p-CFH. Therefore, the experiment was conducted by applying the force F_z in the z-axis direction to the upper finger part to apply a moment to point O. As shown in Figure 3b, CFH fingers and p-CFH fingers are attached to an automatic linear guide that moves in a direction perpendicular to the ground. In both cases, the experiment was performed five times by moving the linear guide in the negative direction of the z-axis and using a load cell to apply the linear load F_z to the upper part of the finger. As a result, the value of F_z was measured according to the displacement of the z-axis, as shown in Figure 3c.

To obtain k_{M_y,θ_y} from the values shown in the graph above, we used geometric values of the deformation that occurred when F_z was applied to a finger. Figure 4a shows the initial state of the finger before force is applied. When F_z is applied to point P' in the initial state, the finger rotates by θ_y around point O, resulting in the state shown in Figure 4b. To obtain the rotational angle θ_y, when $\overline{PP'}=h$ and $\overline{OA}=d$, a relational expression with θ_y must be obtained and can be expressed as $\frac{\overline{AD}}{OA}=sin\theta_y$, $\frac{\overline{AB}}{OA}=tan\theta_y$. In this equation, θ_y has a small value, and so after dividing all three terms of inequality by θ_y and applying them to the limit can be expressed as $k_{M_y,\theta_y}=d^2\frac{F_z}{h}$. The detailed process of obtaining this expression can be found in the part ② of Supplementary Data.

As a result, the value of $\frac{k_{M_y,\,\theta_y}}{d^2}$ indicates the slope of the trend lines in Figure 3c. In both cases of CFH and p-CFH, the force is applied at the same position, and so the moment arm has the same length. Therefore, the ratio of the slope obtained from the trend line becomes the ratio of k_{M_y,θ_y}. Since the slopes of each trend line are 0.0431 and 0.8704, the value of k_{M_y,θ_y} of p-CFH is 20.19 times larger compared with CFH.

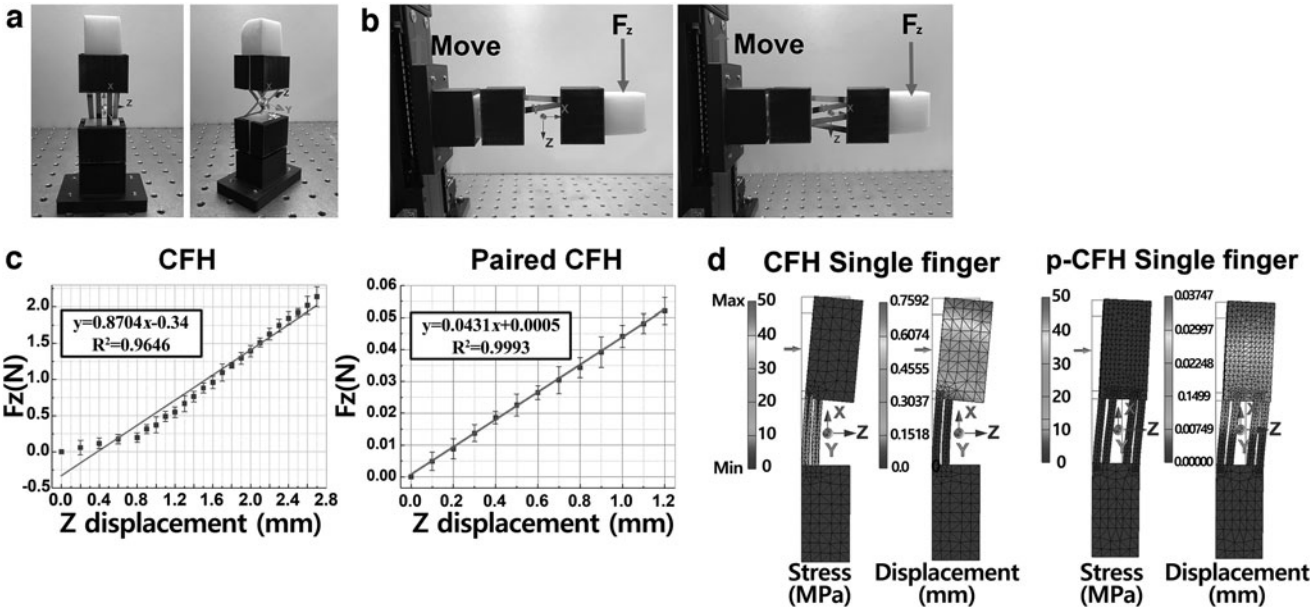

FIG. 3. **(a)** The p-CFH for stiffness experiment. **(b)** Experimental settings for measuring stiffness of CFH and p-CFH. **(c)** The results of force along the z-axis displacement in CFH and p-CFH. **(d)** FEA results for CFH single finger and p-CFH single finger.

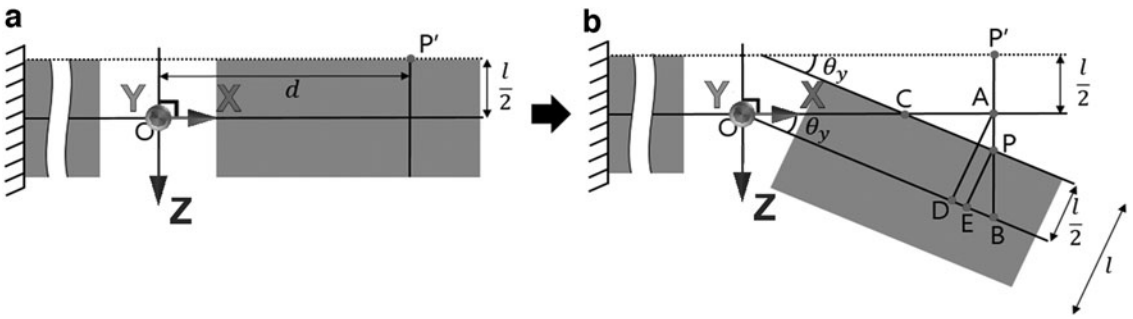

FIG. 4. **(a)** Initial state of the finger. **(b)** Deformation of the finger when applying M_y.

Considering error that occurs during design, the value of 20.19 is similar to the analytical value of 20.28, which is the result calculated using the stiffness matrix component and has an error rate of 0.44%. Therefore, through this experiment, it was confirmed that p-CFH is more suitable than CFH for robot hands because there is no undesired compliance and the supporting stiffness is greatly amplified.

As a final analysis in this section, Finite Element Analysis (FEA) was performed on single fingers made of CFH and p-CFH, respectively. FEA was conducted using AUTODESK INVENTOR (Autodesk, Inc., San Rafael, CA). The material properties of the model applied on the FEA were set to be the same as those of the single finger used in the actual experimental setting. To check $k_{CFH2\_M_y,\theta_y}$ and $k_{CFH\_M_y,\theta_y}$, the bottom of the single finger was fixed in the program, and F_z was applied to the upper part as shown in Figure 3d with the force of 1 N. As a result, the displacement of the CFH single finger was 0.7592 mm (h_1), and the displacement of the p-CFH single finger was generated in the z-axis direction at 0.3747 mm (h_2). The equations related to stiffness of two single fingers can be summarized using $k_{M_y,\theta_y} = d^2 \frac{F_z}{h}$ and expressed as $\frac{h_{CFH}}{h_{CFH2}} = \frac{k_{CFH2\_M_y,\theta_y}}{k_{CFH\_M_y,\theta_y}}$. As a result, if calculated using the displacement identified using FEA, the value of $\frac{h_{CFH}}{h_{CFH2}} = 20.26$ can be obtained. It has an error rate of 20.28 and 0.098%, which are formally confirmed in Eq. (12), and can be said to be similar. In addition, when checking the von Mises stress, it can be visually confirmed that more stress is applied to the hinge of the CFH single finger than the p-CFH single finger. It shows that the p-CFH structure is more suitable for robot hand manufacturing because it is less stressed than the CFH structure.

Design of Anthropomorphic Robot Hand

Overall configuration of robot hand

The robot hand produced in this study is designed to be similar to the structure of a human hand, so that objects of various shapes can be grasped. As shown in Figure 5a, the index, middle, and ring fingers are designed as three phalanges connected by p-CFH. All three fingers are designed in the same shape. The thumb is designed to be twisted 45° relative to the palm, similar to the case of a human hand. And, when viewed from above, the first metacarpal was positioned at an angle of 90° to the other three fingers. One direct current motor is used to move one finger. After fixing the shaft for each finger joint in the empty space between phalanges, the wire was wound around each shaft. When the wire is pulled using the motor located inside the palm, the finger is bent toward the palm, and the robot hand performs grasping. All four fingers of the robot hand have resilience to maintain their hands open due to p-CFH. Therefore, when the torque applied to the motor is released, the hand automatically opens due to the elastic force of p-CFH.

Design of curved p-CFH and phalanges

The p-CFH introduced above has four flat and thin rectangular elastic plates intersecting with each other in a twisted position. When a beam is bent while finger is bent to hold an object, the ability to support the load can rapidly decrease. To solve this problem of supporting stiffness that decreases depending on the angle of rotation, a previous study was conducted to design an Angled Three-Flexure Cross Hinge using an initially curved beam; it was experimentally confirmed that the supporting stiffness increased as the bending angle increased.[26] However, the structure presented in the previous study is not suitable for our robot hand because it is difficult to place a wire inside the finger link. And, when the fingers are unfolded (without deformation in the CFH), they have high supporting stiffness and cannot absorb shock applied in the z-axis direction. To solve these problems, we initially produced CFH with a curved beam shape. Figure 5d shows how the curved p-CFH connects the phalanges of the fingers. The green part in the picture is the polylactide phalanx, produced with a Zortrax M300 3D printer (Zortrax SA, Olsztyn, Poland) using a lamination method. Neighboring phalanges were connected using four curved beams. Both ends of the plate were folded into an L shape and fixed to phalanges so as not to fall out. Carbon structural steel (SK5) was used for the plate, and heat treatment was applied for high elasticity. The performance of the actual gripper model is determined by the size of the hinge, the Young's modulus, and Poisson's ratio among the material properties. In particular, it is highly dependent on the Young's modulus value. Therefore, a material with a large Young's modulus was selected for good performance. The reason for choosing this material is that the larger the value of the Young's modulus of the hinge material, the greater the performance of the actual gripper model. The resilience in each direction is proportional to the Young's modulus of the material, since we selected the material with a large Young's modulus to increase the resilience to perform the hand extension better. In addition, by increasing the Young's modulus, stiffness also

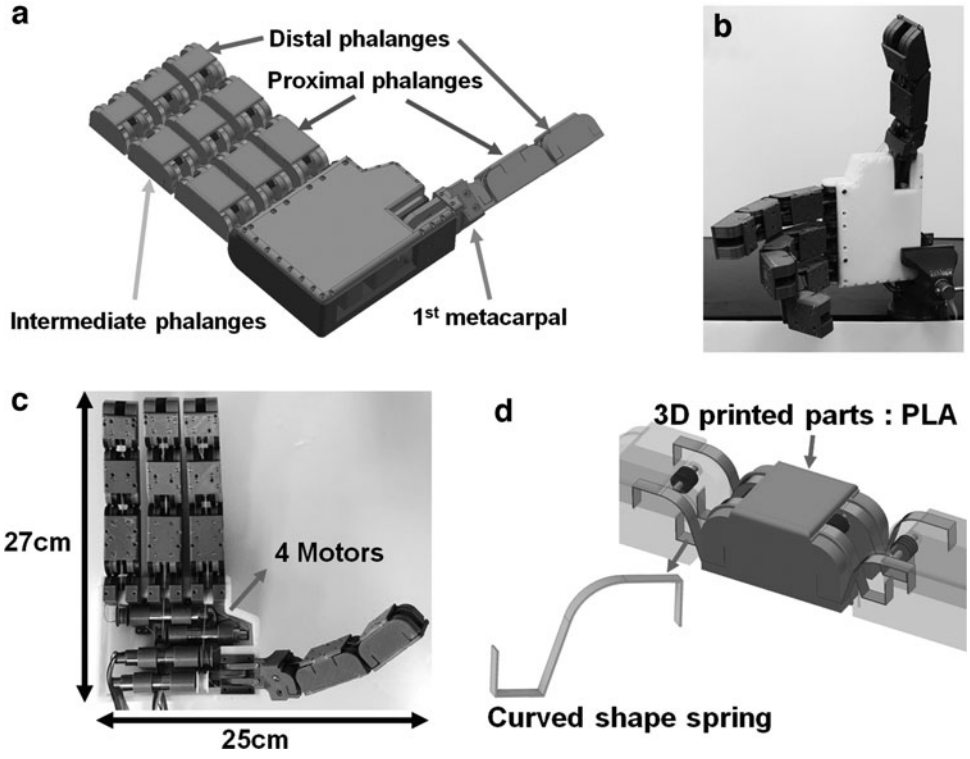

FIG. 5. Configuration of proposed anthropomorphic robot hand. **(a)** Configuration of finger parts. **(b)** Proposed robot hand. **(c)** Top view. **(d)** Components of the phalanges.

increases, thus gripper can get advantages in terms of vibration reduction and shock absorption during impact. For these reasons, a material with a higher Young's modulus was selected, and carbon structural steel (SK5) (GPa) would be more suitable for the actual gripper fabrication than the stainless steel plate (SUS306) used in the experiment (200 GPa).

Figure 6a shows that the gap between the phalanges gradually decreases as the fingers bend to grab the object. The CFH is on the whole curved, but it can be seen that CFH, which appears as a gap, maintains an almost straight shape. Therefore, to prevent the reduction of the supporting stiffness occurring in the curved portion, excluding the straight portion of the CFH, as shown in Figure 6b, the projected portion on the curved surface of the phalanges was made to structurally prevent sagging of the curved section.

If the distance between phalanges decreases, the length (L) of the straight section beam of CFH also decreases. As can be seen in Eq. (11), which shows the supporting stiffness of CFH, as L decreases, the denominator becomes smaller and the supporting stiffness increases. The CFH in the gap is not a perfect straight line, so it is theoretically impossible to determine the stiffness value. Therefore, as shown in Figure 7a,

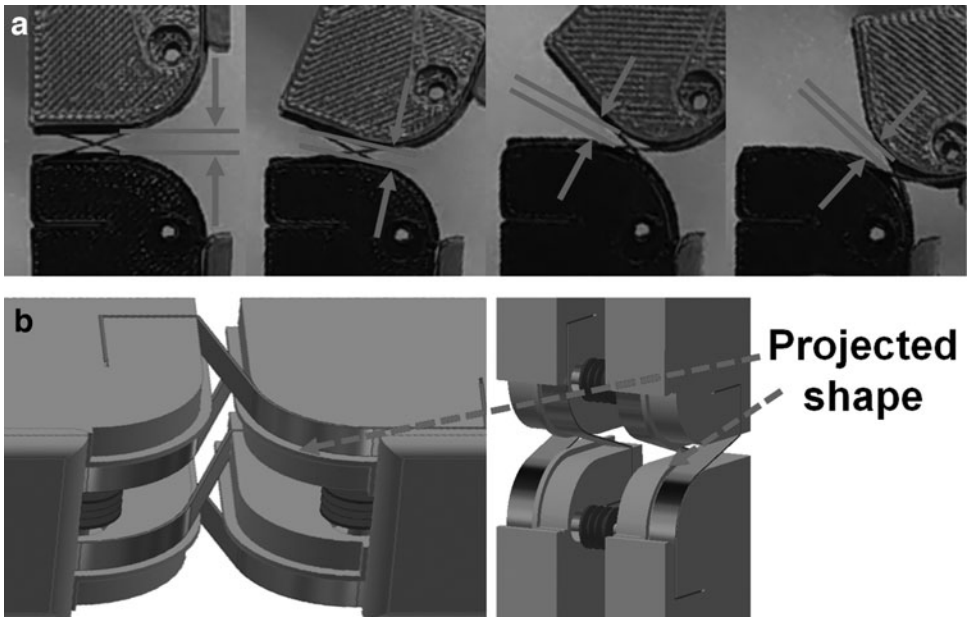

FIG. 6. **(a)** Gap between phalanges gradually decreases. **(b)** Projected shape at *curved plane* of phalanges to prevent the effect of *curved part*.

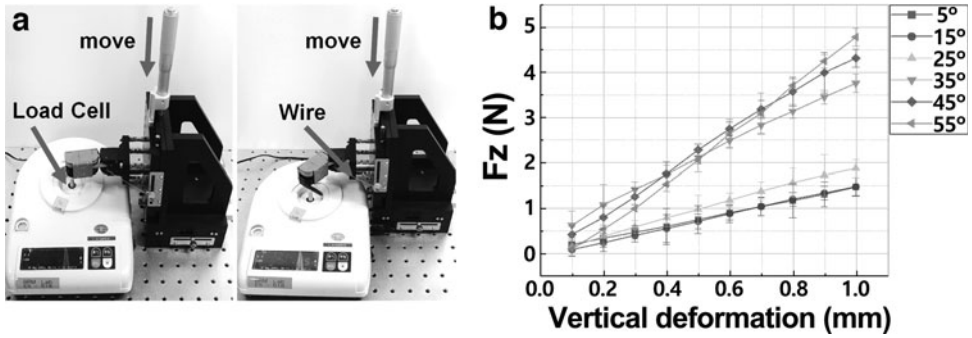

FIG. 7. **(a)** Experimental setting to measure supporting stiffness according to bending angle of finger. **(b)** Measured force with respect to vertical displacement.

it was experimentally confirmed that the supporting stiffness increases while flexing the finger; the experiment to measure the stiffness of one p-CFH joint of the robot finger was repeated five times. The lower phalanx of the finger was fixed to a vertically moving manual linear stage device; the upper phalanx was pushed using a load cell. The shaft was placed in the space between each phalanx, and the bending angle was adjusted by pulling the wire wound around the shaft. While changing the bending angle from 5° (no load state) to 55°, data from the load cell were acquired by moving the stage equipment by 0.1 mm in a vertical downward direction. Figure 7b shows the result for the load value of the load cell, measured according to the bending angle of the one finger. It can be seen from the graph that as the bending angle of the finger increases, the slope, which indicates the supporting stiffness, increases. However, the stiffness does not increase linearly with the bending angle; the reason for this is as follows. First, the length of the beam does not decrease linearly as the bending angle increases. And, because the CFH between phalanges is not a perfect straight line, nonlinear properties exist. When the fingers are bent, the load carrying capacity increases, and so when the object is grasped, the hand can structurally support the load of the object. In addition, when all fingers are fully extended (without using a robot hand), the supporting stiffness is low and the compliance is large and so a certain amount of shock can be absorbed in any direction.

Design of three fingers and underactuated mechanism

The designed robot hand's index, middle, and ring fingers are designed identically. Figure 8b shows the internal structure of these three fingers. Each phalange was connected to another by a curved p-CFH, and grooved pulleys and shafts were installed to wind the wire for actuation. Bearings were attached to both ends of the shaft. The pulley fixed to the distal phalanx was set to No. 1, and the last pulley was set to No. 6. Using a kinematic method, the proposed CFH is unable to precisely control the angle of each joint because the rotation center continuously changes as the finger is bent. Therefore, the underactuated mechanism method, which can bend an entire finger using one motor, was selected. As shown in Figure 8b, the starting point of the wire was firmly fixed to pulley No. 2, then wound halfway around pulley No. 1, and then wound with No. 4 → No. 3 → No. 6 → No. 5 pulleys in order. The end of the wire wound onto the last pulley, No. 5, is securely fixed to the pulley attached to the motor. In the next step, a new mirror-symmetric finger component is attached to an existing finger component with a wire. Then, we put the lid on the palm and back of the hand and fixed them firmly to complete the assembly of one finger. When the motor pulley rotates in the clockwise direction to hold the object, as shown in Figure 8a, the gap between each pulley narrows, and eventually the fingers are bent. If the tension of the wire pulled by the motor is T, the force applied to each shaft is amplified to 2T, and the object can be held in a more robust state. When all joints are fully bent, the motor will stop rotating. Using this mechanism, it is possible to tightly wrap an object of unspecified shape through one rotation of the motor. When the wire is released by applying a reverse rotation to the motor, the fingers spread due to the elasticity of CFH.

Biologically inspired design of thumb

In the case of the thumb, the palm and the metacarpal bone were connected by a ball bearing, and the remaining joints were connected by p-CFH. Figure 9a compares the movement of a human thumb and the movement of a robot thumb when holding a cylindrical object. In humans, the anterior side of the thumb maintains a slight angle to the palm, unlike the other fingers. In power grasp operation, the first metacarpal is folded and the thumb faces the other four fingers, so the hand can stably grasp the object. To implement a stable power grasp like that of a human, the robot's thumb was designed as shown in

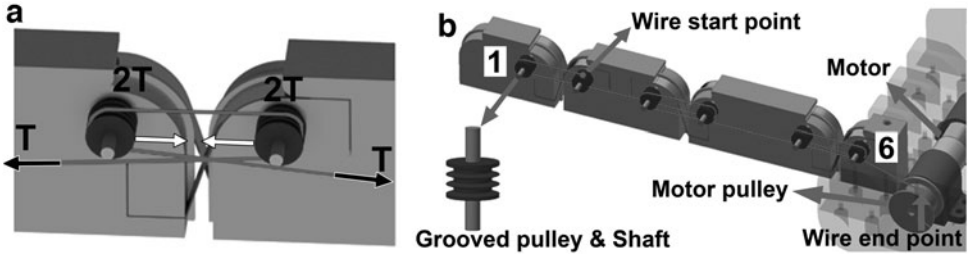

FIG. 8. **(a)** Tension of the wire applied to the pulley. **(b)** Structure of three fingers and placement of wire.

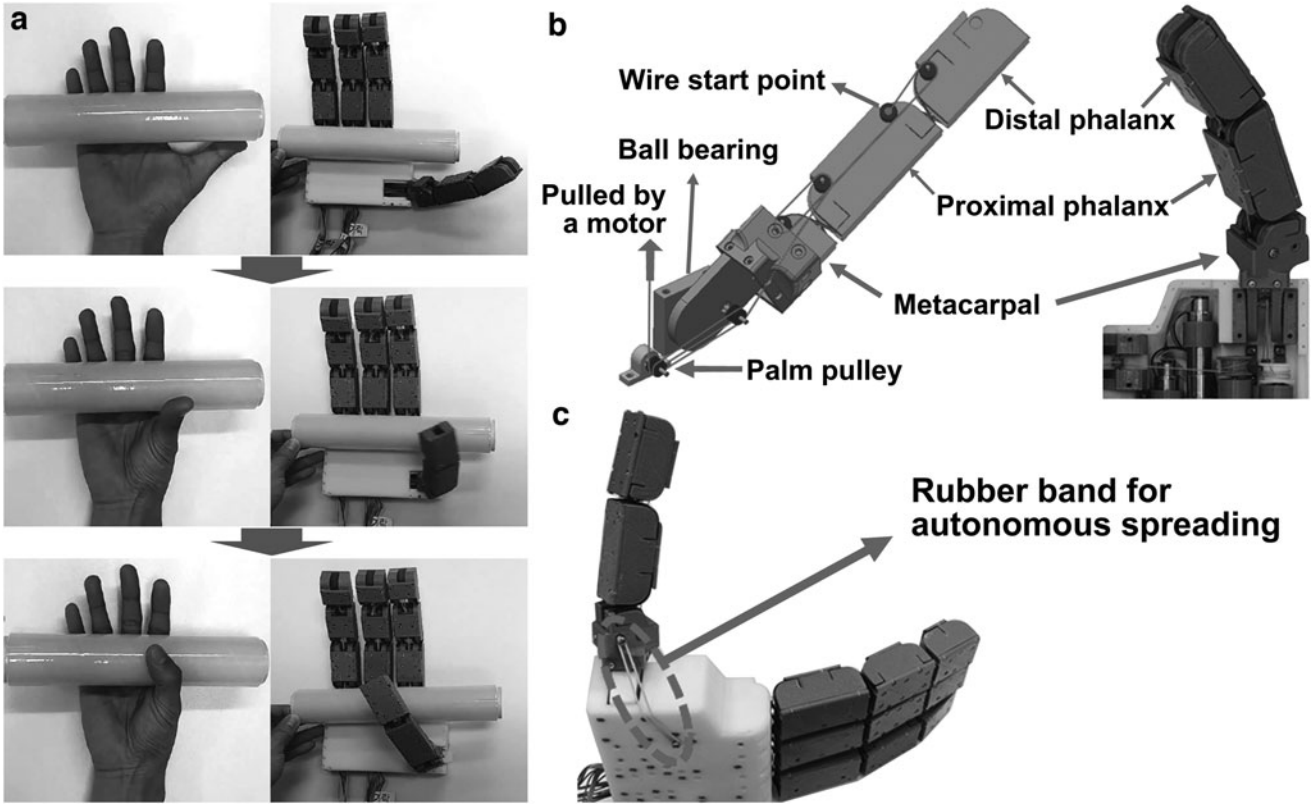

FIG. 9. **(a)** Bending procedure of human thumb and the robot hand. **(b)** Structure of thumb and placement of wire. **(c)** Rubber band that connects palm and metacarpal.

Figure 9b. The first joint of the thumb was installed 90° away from the other joint. As a result, unique gripping motion of the thumb could be achieved with a single motor. The wire was wound around the distal proximal phalanx of the thumb, and the pulleys of the metacarpal, in the same way as for the index, middle, and ring fingers. Finally, the wire was wound around the metacarpal pulley and palm pulley for rotation of the metacarpal. Among the phalanges, the metacarpal pulley and palm pulley were wound twice by amplifying the bending moment so that the metacarpal was bent first. When extending the hand, a rubber band was tightly connected to the metacarpal and the back of the hand, as shown in Figure 9c, so that it could be restored elastically, like the other fingers. When the motor was driven in the reverse direction in the operation of releasing the object, the thumb returned to the initial state due to the elasticity of the CFH and the rubber band.

Experiments and Results

Grasping test

We conducted experiments to see if the robot hand can hold objects of various shapes, sizes, and weights, how increased supporting stiffness affects grasping, and how heavy objects of a particular shape can be lifted. In the experiment, 0.3A, which is less than half of the rated current of 0.649A, was set as the input current limit to prevent damage to the motor when the robot hand was holding the object.

First, as shown in Figure 10a–i, it was confirmed that the robot can grasp objects of various shapes well. The robot hand was fixed to a table so that the palm face was perpendicular to the ground, and power was applied to hold the object. Since the supply current was limited to 0.3A, the grasping operation ended when the applied current reached 0.3A. For diversity of shapes, nine objects with different shapes were selected, and it was confirmed that all selected objects could be held firmly.

In the second experiment, we examined whether increasing supporting stiffness when bending a finger actually contributed to load carrying capacity. As shown in Figure 10j, when a 2 kg mass bolt pack was used, the lower ring finger was bent to the maximum to stably support the load of the object. If the supporting stiffness had not increased, it would not have been possible to perform stable operation due to the sagging of the finger caused by load of the object.

The third experiment measured the maximum load capacity when applying a current close to the rated current to the robot hand. As shown in Figure 10k, a plastic bag was connected to a cylindrical object, and a weight was added. After adding additional weights, the total mass of the object at the moment of sliding from the robot hand was measured. In this experiment, to prevent the motor from being damaged, 0.57A lower than the rated current of 0.649A was used as the supply current. It was confirmed that the maximum mass of 4.041 kg can be supported when power of 12V and 0.57A is applied.

Impact test

In this section, the impact test was carried out in qualitative and quantitative experiments. A qualitative experiment is to check whether the robot hand absorbs shock well when it is not working. After the robot hand was firmly fixed to the

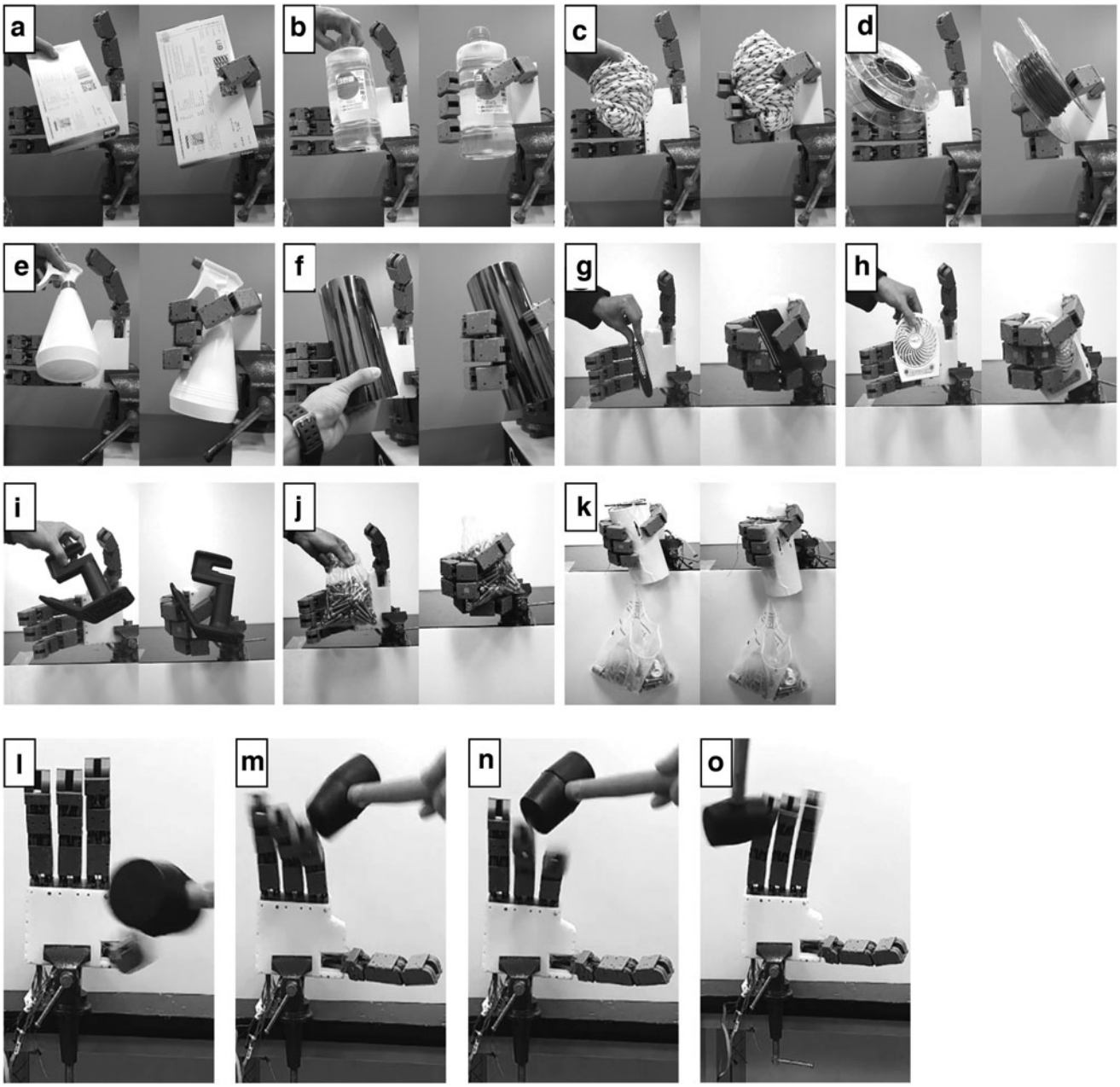

FIG. 10. Grasping test with various shaped objects **(a)** Rectangular tissue box. **(b)** Water bottle. **(c)** A bundle of rope. **(d)** PLA filament disk. **(e)** Spray gun. **(f)** Cylindrical object. **(g)** Wallet. **(h)** Mini fan. **(i)** Plastic structure. **(j)** Grasp 2 kg bag with enhanced supporting stiffness. **(k)** Cylindrical object payload test. **(l-o)** Qualitative impact test using a hammer to strike a robot hand. PLA, polylactide.

desk, using a rubber mallet, impact force was applied in various directions to all fingers. Figure 10l–o shows the instantaneous deformation of the robot hand when impact is applied. As a result, it was confirmed that all impacts can be well absorbed due to the high compliance of the robot hand. In particular, as shown in Figure 10o, the robot hand developed in this study has the ability to absorb sideways impacts that cannot be absorbed by robots made of rigid links and pin joints. When the robot hand is designed with rigid links and pin joints, there is no sideways compliance, and so there is a high risk of damage due to sideways impact transmitted to the body of the robot.

The second impact test is a quantitative experiment, and to perform the experiment, a pin joint model as a control was constructed as shown in Figure 11a. The pin joint model is the most basic method of connecting links among mechanical parts. This pin joint robot hand was made similar to the pin joint structure used in the previous study.[2–4] As shown in Figure 11c, a pin joint structure was used to connect four nodes to one finger, and it was manufactured so that there was no gap using three link connecting parts. The driving method adopts the same wire actuation. Unlike the anthropomorphic robot hand, two sets of wires were applied to the pin joint because the wire must be wound in the opposite direction to

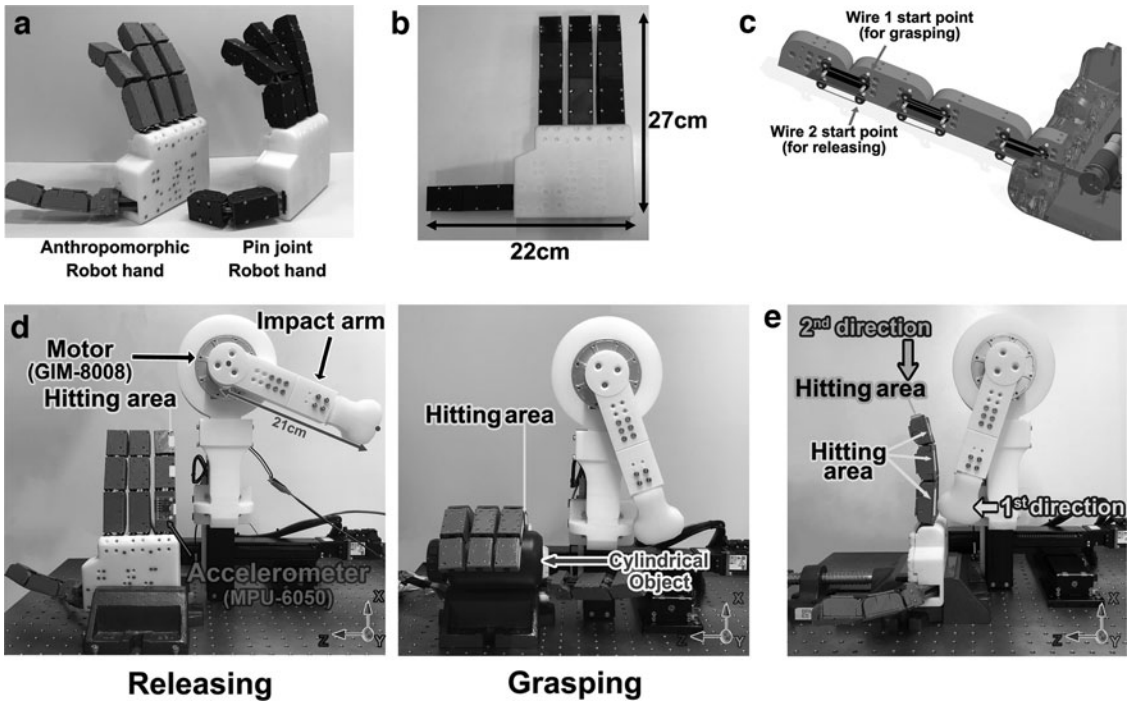

FIG. 11. **(a)** Pin joint robot hand designed for impact test. **(b)** The height and width of the pin joint robot hand. **(c)** Structure of pin joint finger and placement of a pair of wires. **(d)** Experimental settings for quantitative impact test at releasing and grasping state. **(e)** Experimental settings for first and second direction.

grasping to perform releasing. The overall length is 27 cm high and 22 cm wide, as shown in the frontal view of pin joint model in Figure 11b. There is a difference of 3 cm in the thumb width of the pin joint robot hand and the anthropomorphic robot hand made using the p-CFH. The reason is that the anthropomorphic robot hand has the first metacarpal bone implemented to perform grasping similar to the human hand. In contrast, the pin joint model was manufactured according to the existing research method, so the thumb of the pin joint model does not work similarly to the human thumb. It was manufactured by unifying all other conditions except the pin joint structure. The anthropomorphic robot hand weighs 910.7 g and the pin joint model 914.2 g, which has an error of 0.38% when comparing the total weight of the model.

In this experiment, the head injury criterion (HIC) was used to quantitatively measure the amount of impact. HIC is one of the most widely used severity indices for measuring head injuries in many fields, such as vehicles and machinery. The HIC is defined as follows[28]:

$$HIC_{\Delta t_{max}} = \Delta t_{max}\left[\frac{1}{\Delta t_{max}}\int_{t_1}^{t_2} \hat{a}\ dt\right]^{2.5} \qquad (13)$$
$$\Delta t_{max} = t_2 - t_1$$

In Eq. (13), $\hat{a}$ is the value obtained by dividing the actual acceleration data measured at the center of the impact by the gravitational constant ($g = 9.81 m/s^2$). Δt_{max} means the interval between t_2 and t_1 in the acceleration data graph. The most commonly used HIC in the impact test are HIC_{15} and HIC_{36} using $\Delta t_{max} = 15ms$ and $\Delta t_{max} = 36ms$. There is a prior study that conducted an impact test using HIC in a robot system.[29–31] Therefore, in the second impact test, a quantitative experiment was performed to compare the HIC_{36} value by applying the same amount of impact to the anthropomorphic robot hand proposed in this study and the pin joint robot hand as a control model. As shown in Figure 11d, an impact arm with a silicone-covered end was connected to the motor GIM8008 (Skyline Innovation Co., Limited, Nanchang, China). The motor was connected to a 3-DOF stage for height adjustment, and the experimental environment was set to hit the center side of the proximal phalanges, intermediate phalanges, and distal phalanges as a hitting area. Since the input torque of the motor is 0.5 Nm and the length of the impact arm is 21 cm, the force applied to the finger vertically at the end of the impact arm is 2.38 N. A 3-axis gyro and acceleration sensor, MPU-6050 (InvenSense, San Jose, CA), was installed inside the finger joint to obtain acceleration data when it was impacted by the impact arm. The sampling frequency of the sensor is set to be 250 Hz. The quantitative experiment was conducted in two cases, the releasing state and the grasping state. For each state, it was performed seven times for each node, and a total of 21 shocks were applied to the anthropomorphic and pin-jointed robot hands by changing the hitting area.

The acceleration graph obtained when the two models are impacted using an impact arm for both conditions is shown in Figure 12a and b. The acceleration expressed in both graphs means the value of the z-axis direction equal to the direction in which the impact arm hits vertically. The blue area in the graph represents the area corresponding to HIC_{36}. First, the amount of impact when the two robot hands are in the releasing state was compared. In the acceleration graph of the anthropomorphic robot hand proposed in this study, the maximum value of 4.23 g in the proximal hitting area is shown as the peak value, and the average peak value is 3.18 g.

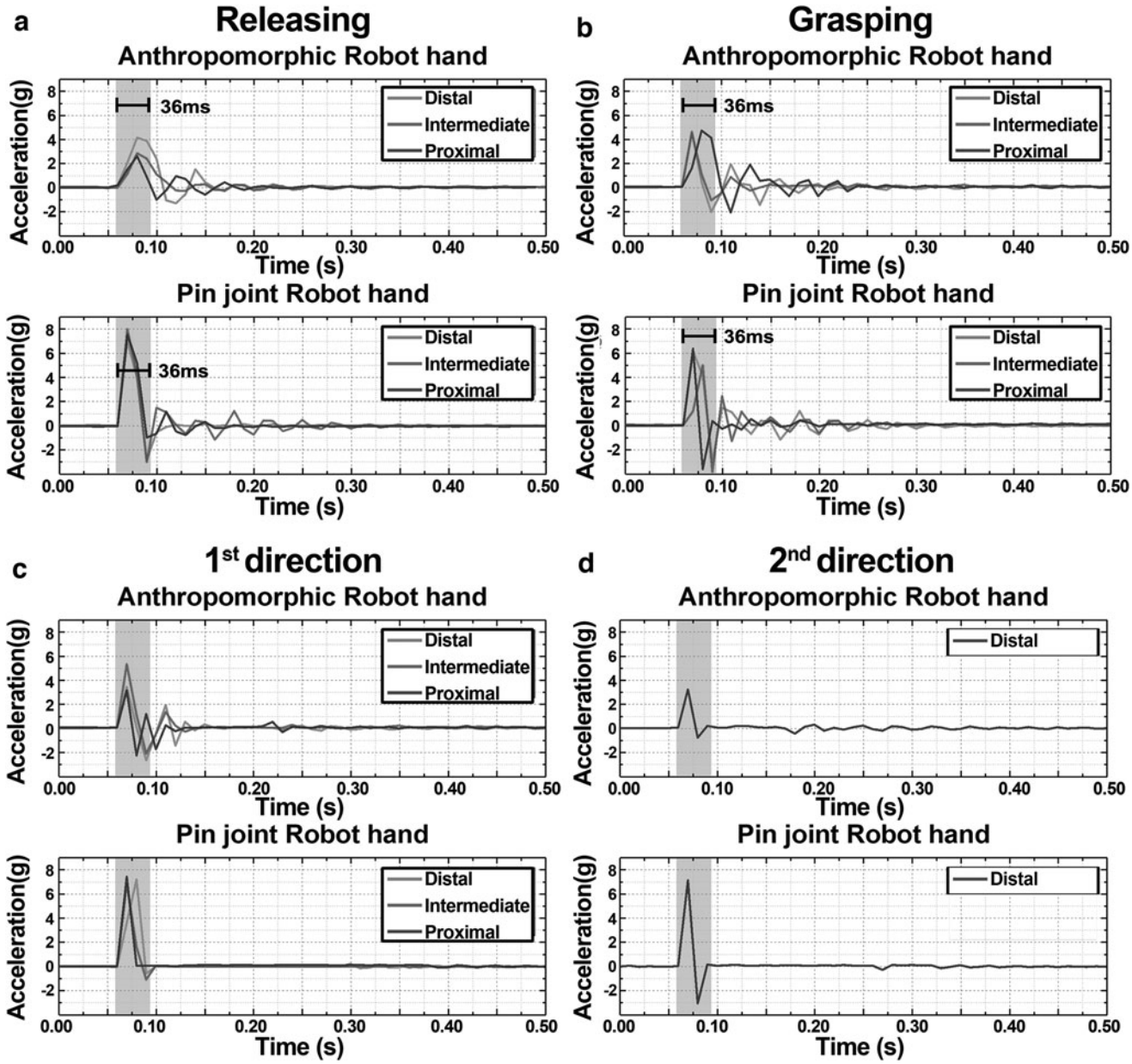

FIG. 12. **(a)** Acceleration graph through impact test in releasing state. **(b)** Acceleration graph in grasping state. **(c, d)** Results of first and second direction.

The average time after reaching the first peak until reaching the negative peak value is 0.048 s. In the acceleration graph of the pin joint robot hand, the peak value was 7.97 g in the intermediate hitting area, the middle node of the finger, and the average peak value was obtained as 7.54 g. The average time between the first peak and the negative peak is 0.023 s. When comparing the average accelerations of the two models, a 57.82% reduction in acceleration was measured in the anthropomorphic robot hand. The anthropomorphic robot hand's HIC_{36} values were $0.3227m^{5/2}s^{-4}$ at proximal, $0.0685m^{5/2}s^{-4}$ at intermediate, and $0.0973m^{5/2}s^{-4}$ at distal. And the pin joint robot hand is $0.4774m^{5/2}s^{-4}$, $0.7199m^{5/2}s^{-4}$, $0.3049m^{5/2}s^{-4}$, respectively, in the same order. Comparing the average HIC_{36} of the three nodes, the anthropomorphic robot hand decreased by 67.48% compared to the pin joint robot hand. Next, the amount of impact when the two robot hands are grasping was compared. When both robot hands performed grasping, the experiment was conducted under the same conditions, and a cylindrical object was used. The hitting area was kept the same as in the previous experiment, and as a result, the average peak value of the acceleration graph was 4.62 g in the anthropomorphic robot hand. Compared with the average acceleration value of the pin joint robot hand with 5.81 g, it was confirmed that it was reduced by 20.51% in the anthropomorphic robot hand. When the HIC_{36} value was calculated by the same method as the releasing state experiment, it was confirmed that the HIC_{36} value of the anthropomorphic robot hand was reduced by 26.98% compared to the pin joint robot hand. In addition, the impact test was conducted by setting

new directions, first direction and second direction, as shown in Figure 11e, excluding *z*-axis, which is the direction of the previous experiment. The direction of the impact test conducted earlier was *z*-axis based on the robot hand model. In this experiment, the robot hand model was rotated and installed on the stage, and then the first direction was set in the same direction as the *y*-axis and the second direction was set in the same direction as the *x*-axis. As a result, the HIC_{36} value decreased in the anthropomorphic robot hand compared with the pin joint model. It was confirmed that the decrease was 58.36% in the first direction and 33.86% in the second direction.

This shows that the robot hand using p-CFH can absorb the shock in all axial directions better than the robot hand with a pin joint structure. The reason why the robot hand using the p-CFH structure can absorb shock is that there is no undesired compliance, so the load carrying capacity in the *z*-axis direction is excellent as shown in Figure 3c. In addition, what was confirmed in the acceleration graph of the anthropomorphic robot hand in Figure 12a is that it takes about 2.08 times more time to reach the negative peak from the positive peak to reduce the impact than the pin joint robot hand after the impact. This is because the finger of the robot hand vibrates in response to the impact along the *z*-axis rather than the pin joint, which allows the p-CFH structure to have a high impact absorption rate.

Conclusion

In this study, a curved p-CFH structure was applied to a robot hand, and a mechanism for maximizing the advantages of the flexure hinge was designed to implement an anthropomorphic robot hand that is strong against impact and has enhanced payload. Because its rotation center is relatively well defined compared to those of other flexure hinges, and its supporting stiffness is relatively large, CFH has been used as a revolute joint to replace ball bearings. Using the CFH structure has the advantage that the design and assembly process can be simplified, and research has been conducted to apply it to the design of a robot hand. In this study, a p-CFH structure is proposed to increase the load capacity and to eliminate the undesired compliance that occurs when CFH is applied to robot hands. Using a 6×6 stiffness matrix for p-CFH, it was theoretically confirmed that the supporting stiffness is significantly higher compared with conventional CFH; this was also experimentally verified. The robot hand was designed using the proposed joint, and p-CFH was initially composed of curved plates to increase the supporting stiffness as the fingers were bent. The robot hand is driven by an underactuated wire mechanism, and one finger is driven by one motor. This has the advantage of allowing objects of various shapes to be lifted without a complicated control algorithm. To hold an object stably, as by the human power grasp, the finger placement of the robot hand was made similar to that of the human hand. In particular, a new structure was proposed and designed so that the thumb can implement a movement similar to that of a human thumb. Finally, it was experimentally confirmed that the developed robot hand can achieve the desired performance. As a final experiment, qualitative and quantitative impact test were performed. In the qualitative impact test, the external impact force was applied in an unspecified direction when the robot was not being driven, and it was confirmed that the robot hand can absorb external impact due to its inherent compliance. In the quantitative impact test, an impact arm was designed to create an experimental environment capable of applying a constant force. As a result, the amount of shock absorption applied in the *z*-axis direction when the two models are in a releasing state and in a grasping state was confirmed using HIC. In addition, the quantitative impact test in the other two directions was conducted under the same conditions. The contribution points of this study are as follows. The nondiagonal component generated in the theoretical stiffness analysis conducted in this study was eliminated using the p-CFH structure. In addition, by designing the anthropomorphic robot hand through the shape and structural transformation of the p-CFH, the load carrying capacity of the rigid pin joint-based robot hand and the shock absorbing capability of the fully-compliant robot hand were simultaneously enhanced.

Several future works need to be done to solve some of the limitations that are not solved in this study. First, it is necessary to attempt to find a material suitable for the robot hand by changing the materials constituting p-CFH. In addition to the materials used in this study, after performing modeling using various materials, it is necessary to find and propose a more suitable material through FEM analysis. If the p-CFH structure or robot hand model manufactured for each material is compared, the most efficient p-CFH robot hand can be manufactured. As a follow-up to the grasping experiment performed in this study, it is necessary to conduct an experiment to measure the maximum number of grasping so that the lifetime of p-CFH can be confirmed. In addition, it is necessary to design the experiment with reference to the related study to modify the strength and test lifetime for the carbon structural steel, which is used to fabricate the p-CFH of this study.[32,33] It is an experiment that must be performed to confirm how continuously the newly proposed p-CFH robot hand can be used. Finally, as a follow-up to the quantitative impact test, it is necessary to conduct experiments with different impact amounts and analyze the impact absorption rate of the robot hand. An experiment to check the threshold value of the maximum absorbable impact amount of the robot hand should be accompanied.

Author Disclosure Statement

No competing financial interests exist.

Funding Information

This work was supported by the National Research Foundation of Korea (NRF) grant funded by the Korea government (MSIT) (No. 2020R1C1C1012279).

Supplementary Material

Supplementary Data

References

1. Xiong C, Chen W, Sun B, *et al.* Design and implementation of an anthropomorphic hand for replicating human grasping functions. IEEE Trans Rob 2016;32:652–671.
2. Kawasaki H, Komatsu T, Uchiyama K. Dexterous anthropomorphic robot hand with distributed tactile sensor: Gifu Hand II. IEEE/ASME Trans Mechatron 2002;7:296–303.

3. Roccella S, Carrozza MC, Cappiello G, *et al.* Design, fabrication and preliminary results of a novel anthropomorphic hand for humanoid robotics: RCH-1. In: 2004 IEEE/RSJ International Conference on Intelligent Robots and Systems (IROS) (IEEE Cat. No. 04CH37566), September 28–October 2, Sendai, Japan. 2004, Vol. 1, pp. 266–271. IEEE.
4. Takamuku S, Fukuda A, Hosoda K. Repetitive grasping with anthropomorphic skin-covered hand enables robust haptic recognition. In: 2008 IEEE/RSJ International Conference on Intelligent Robots and Systems, September 22–26, Nice, France. 2008, pp. 3212–3217. IEEE.
5. Atasoy A, Toptas E, Kuchimov S, *et al.* Biomechanical design of an anthropomorphic prosthetic hand. In: 2018 7th IEEE International Conference on Biomedical Robotics and Biomechatronics (Biorob), August 26–29, Enschede, Netherlands. 2018, pp. 732–736. IEEE.
6. Batsuren K, Yun D. Soft robotic gripper with chambered fingers for performing in-hand manipulation. NATO Adv Sci Inst Ser E Appl Sci 2019;9:2967.
7. Deimel R, Brock O. A novel type of compliant and underactuated robotic hand for dexterous grasping. Int J Rob Res 2016;35:161–185.
8. Yamaguchi T, Kashiwagi T, Arie T. Human-like electronic skin-integrated soft robotic hand. Adv Intell 2019;1:1900018.
9. Zhou J, Yi J, Chen X, *et al.* BCL-13: A 13-DOF soft robotic hand for dexterous grasping and in-hand manipulation. IEEE Robot Autom Lett 2018;3:3379–3386.
10. Ho V, Hirai S. Design and analysis of a soft-fingered hand with contact feedback. IEEE Robot Autom Lett 2017;2:491–498.
11. Shahid Z, Glatman AL, Ryu SC. Design of a soft composite finger with adjustable joint stiffness. Soft Robot 2019;6:722–732.
12. Zhao S, Bi S, Yu J, *et al.* A large-deflection annulus-shape flexure hinge based on curved beams. In: ASME 2008 International Design Engineering Technical Conferences and Computers and Information in Engineering Conference, August 3–6, Brooklyn, NY. 2009, pp. 249–255. ASME.
13. Tielen V, Bellouard Y. Three-dimensional glass monolithic micro-flexure fabricated by femtosecond laser exposure and chemical etching. Micromachines 2014;5:697–710.
14. Mohd Zubir MN, Shirinzadeh B. Development of a high precision flexure-based microgripper. Precis Eng 2009;33:362–370.
15. Polit S, Dong J. Design of high-bandwidth high-precision flexure-based nanopositioning modules. J Manuf Syst 2009;28:71–77.
16. Lin R, Li Y, Zhang Y, *et al.* Design of a flexure-based mixed-kinematic XY high-precision positioning platform with large range. Mech Mach Theory 2019;142:103609.
17. Mutlu R, Alici G, in het Panhuis M, *et al.* 3D printed flexure hinges for soft monolithic prosthetic fingers. Soft Robot 2016;3:120–133.
18. Odhner LU, Jentoft LP, Claffee MR, *et al.* A compliant, underactuated hand for robust manipulation. Int J Rob Res 2014;33:736–752.
19. Jensen BD, Howell LL. The modeling of cross-axis flexural pivots. Mech Mach Theory 2002;37:461–476.
20. Zhao H, Bi S. Stiffness and stress characteristics of the generalized cross-spring pivot. Mech Mach Theory 2010;45:378–391.
21. Marković K, Zelenika S. Optimized cross-spring pivot configurations with minimized parasitic shifts and stiffness variations investigated via nonlinear FEA. Mech Based Design Struct Mach 2017;45:380–394.
22. Hongzhe Z, Shusheng B. Accuracy characteristics of the generalized cross-spring pivot. Mech Mach Theory 2010;45:1434–1448.
23. Wittrick WH. The properties of crossed flexure pivots, and the influence of the point at which the strips cross. Aeronaut Quart 1951;2:272–292.
24. Yi Z, Yangmin L. A new method to design robotic hand based on cross-axis flexural pivots. In: Proceedings of the 31st Chinese Control Conference, July 25–27, Hefei, China. 2012, pp. 5129–5134. IEEE.
25. Bellouard Y. Microrobotics: Methods and Applications. Boca Raton, Florida, United States: CRC Press, 2009.
26. Bai G, Rojas N. Self-adaptive monolithic anthropomorphic finger with teeth-guided compliant cross-four-bar joints for underactuated hands. In: 2018 IEEE-RAS 18th International Conference on Humanoid Robots (Humanoids), November 6–9, Beijing, China. 2018, pp. 145–152. IEEE.
27. Garcia L, Naves M, Brouwer DM. 3D-printed flexure-based finger joints for anthropomorphic hands. In: 2018 IEEE/RSJ International Conference on Intelligent Robots and Systems (IROS), October 1–5, Madrid, Spain. 2018, pp. 1437–1442. IEEE.
28. Versace J. A review of the severity index. SAE Technical Paper No. 710881, 1971.
29. She Y, Su HJ, Lai C, *et al.* Design and prototype of a tunable stiffness arm for safe human-robot interaction. In: ASME 2016 International Design Engineering Technical Conferences and Computers and Information in Engineering Conference, August 21–24, Charlotte. 2016, p. 9. ASME.
30. Hyun D, Yang HS, Park J, *et al.* Variable stiffness mechanism for human-friendly robots. Mech Mach Theory 2010;45:880–897.
31. Gao D, Wampler CW. Head injury criterion. IEEE Robot Autom Magaz 2009;16:71–74.
32. Nip KH, Gardner L, Davies CM, *et al.* Extremely low cycle fatigue tests on structural carbon steel and stainless steel. J Construct Steel Res 2010;66:96–110.
33. Yadav D, Gaikwad A. Comparison and testing of tensile strength for low & medium carbon steel. Int J Mech Eng 2015;4:8.

Address correspondence to:
Dongwon Yun
Department of Robotics Engineering
Daegu Gyeongbuk Institute of Science and Technology (DGIST)
Daegu 711-873
South Korea

E-mail: mech@dgist.ac.kr